On the effects of powder morphology on the post-comminution ballistic strength of ceramics

G. J. Appleby-Thomas[1], D. C. Wood[1], A. Hameed[1], J. Painter[1] and B. Fitzmaurice[1]

[1]Centre for Defence Engineering, Cranfield University, Defence Academy of the United Kingdom, Shrivenham, SN6 8LA, UK

Abstract

In this paper in order to try and elucidate the effects of particle morphology on ballistic response of comminuted systems, a series of experiments were carried out-via the use of powder compacts with differing initial particle morphologies. This approach provided a route to readily manufacture comminuted armour analogues with significantly different microstructural compositions. In this study pre-formed `fragmented-ceramic' analogues were cold-pressed using plasma-spray alumina powders with two differing initial morphologies (angular and spherical). These compacts were then impacted using 7.62-mm FFV AP (Förenade Fabriksverken Armour Piercing) rounds with the subsequent depth-of-penetration of the impacting projectile into backing Al 6082 blocks used to provide a measure of pressed ceramic ballistic response. When material areal density was accounted for via differing ballistic efficiency calculations a strong indication of particle morphology influence on post-impact ceramic properties was apparent. These results were reinforced by a separate small series of plate-impact experiments, whose results indicated that powder morphology had a strong influence on the nature of compact collapse.

Keywords: Ballistic penetration; comminuted ceramic; ballistic resistance; plate impact

1. Introduction

Ceramics materials have found an important role in armour applications due to their combination of high hardness and low density [1, 2, 3]. When a projectile impacts a target it imparts a compressive impulse to the material; however on reaching a free surface or an interface with a material of lower impedance, such a compressive wave will be reflected as a tensile pulse. This initial compressive wave (typically consisting of a precursor elastic wave and a trailing stress wave or shock) will fracture the ceramic. Thus, the slower-moving penetrator typically travels into pre-damaged material [2]. As ceramics are extremely strong in compression, but weak in tension [4], control of the stress state is of core importance in their use as an armour material.

Four stages are typically involved in the penetration of a ceramic armour located on an absorbing backing material [1]. These comprise: (1) overmatch – when the ceramic is inherently stronger than the projectile and surface-defeat (dwell) occurs; (2) initial penetration – which occurs when a cone of comminuted (crushed) material forms ahead of the projectile, with the steadily decreasing size of the comminuted material increasing pressure both on the backing and radially (a process known as bulking, due to the greater volume of the fractured material); (3) flexure of the backing, and finally; (4) failure of the backing layer – typically via plugging or a similar mechanism.

The inherent flaws present within ceramic materials (e.g. pores, micro cracks and grain boundaries) which lead to their brittle nature [5] act as stress concentrators during both compressive and tensile loading. Despite the aforementioned comminution on initial loading, crack propagation will be inhibited until arrival of tensile releases provides an opportunity for micro fracture to occur – leading to material failure [6]. Despite a rapid decrease in target strength during the initial penetration phase, as fracture of the ceramic occurs, several studies

which have shown that this comminuted material – on further compaction – then provides a residual resisting strength with respect to penetration [7, 8, 9]. The concept of ballistic strength discussed in this paper is essentially a measure of the ability of armour to resist penetration following an impact event. A number of different approaches – both experimental and computational – have been adopted to investigate such material response, with the ultimate aim of allowing improved armour (or munition) development from the resultant insight into armour behaviour.

Holmquist et al. [10] undertook a series of experiments to investigate the defeat mechanisms for SiC tiles impacted in a reverse ballistics configuration by 1-mm diameter Au long rods. By monitoring a variety of impact events via a flash X-ray system the authors were able to discern both the onset of the dwell-penetration transition and the nature of subsequent penetration. Interestingly, a non-linear penetration velocity was discerned in all cases, in line with computational simulations. This behaviour was attributed to the multi-stage nature of the ceramic failure – with impacted material being comminuted before penetration occurred. However, in this study the nature of this comminuted material – and its precise contribution to ballistic resistance – were not discussed – something which will be investigated here.

A recent study by Horsfall et al. [11] however, focused to a greater extent on the contribution of fractured materials. In this study Sintox® FA tiles comprising 95% alumina were explosively comminuted within a confining steel frame. An in-situ Al 7018-T6 witness plate located directly beneath the tile allowed subsequent depth-of-penetration (DOP) testing [1, 12, 13, 14] without further disturbance of the comminuted material. Further, as a comparison, 80 µm pure alumina powder was pressed in-situ in identical confinement rigs to 67% of theoretical density. Ballistic tests were carried out on two different thicknesses of powder layup using 7.62 mm FFV rounds at ~950 m/s. While the ballistic resistance was

reduced, the explosively shattered material was still found to provide a significant resistance to penetration, shattering the core – whereas the pressed material had a less marked effect. This poorer performance for the powder compacts was tentatively attributed by the authors to both a relative lack of confinement and – more significantly in the context of the current study – the fact that the pressed powder had a spherical morphology which would have minimised frictional effects during compression. It was suggested that this difference in morphology might be partially responsible for the enhanced behaviour of the shattered tiles which possessed an angular microstructure; further, it was pointed out that the shattered tiles are analogous to the state which the intact tiles would enter shortly after impact.

Building on this work, Nanda et al. [7] employed an identical confinement rig to allow a variety of different ceramic materials to be explosively shattered before being subjected to depth-of-penetration testing. Experimental results indicated little difference in the subsequent ballistic mass efficiency (E_m; a comparison of the ballistic efficiency of the ceramic + backing to the backing alone [4]), despite substantially different initial ceramic strengths. Differing explosive loads were used to shatter the different ceramics. However, in line with concepts / conclusions presented elsewhere [10, 11], the relative independence of E_m from material type was taken to suggest that the ballistic resistance provided by the shattered material was dependant on the form of the particles (morphology), rather than the material's strength. This seems a reasonable conclusion given that all three materials were shattered in a similar manner – however unlike the work by Horsfall et al. [11] no systematic study of the effects of this explosive loading on microstructure were undertaken.

More recently, building on both ballistic tests and data from the literature, Hazell et al. [15] developed a constitutive model to predict the ballistic response of ceramic powder compacts. Simulations in ANSYS Autodyn® were able to successfully model experimentally measured penetration of projectiles into differing powder compacts with the core assumption of a

4

pressure-dependant material compaction. However, while the simulations proved efficient at predicting the ballistic response of angular compacts, they proved less efficient with spheroidized feedstock materials (data from the literature), with differences of approximately 12% between simulation and experiment. It was also of note that the validation experiments reported in this work only found relatively low mass efficiencies of $E_m \sim 1$ for the powder compacts under test. Overall, these simulations, while useful, were insufficient to fully elucidate the contribution of particle morphology to resultant ballistic response in comminuted ceramics. Consequently, experimental investigation – as conducted in this study – is of paramount importance in this sphere.

Bourne [9] has also investigated the ballistic strength of ceramics. However, unlike the ballistic-based approaches to assessment of comminuted ceramic strength detailed above [7, 10, 11], this work focused on direct measurement of the strength of shocked ceramic (AD995 alumina). This was achieved by loading ceramic materials into a one-dimensional state of strain (but not stress) via the plate-impact technique [16, 17, 18]. Embedded longitudinal and lateral stress gauges were employed to determine the variation in stress in both the longitudinal (σ_x) and transverse (σ_y) directions, allowing calculation of the variation in shear strength (τ) behind the shock via the relation $2\tau = \sigma_x - \sigma_y$. From these in-situ measurements and corresponding soft recovery of shocked targets, Bourne found evidence of a substantive change in material response in the first 500 ns due to both twinning and trans- and inter-granular cracking. Further, depth-of-penetration results were found to scale with measured material strength. Taken together, these results appeared to suggest that the early-stage ceramic response has a substantive impact on subsequent ceramic ballistic behaviour; confirming the hypothesis that knowledge of the strength of failed material is of paramount importance in the predication of ceramic ballistic response.

Despite the large body of evidence that it is the comminuted material which controls penetration into ceramic systems, there is limited data on the influence of comminuted microstructure. While several authors [7, 9, 10] have postulated that microstructure plays a key role, few investigators have focused specifically on what attributes of comminuted material (microstructure, porosity, etc) affect the subsequent ballistic response. The aim of this paper is to determine whether comminuted material morphology has an effect on the ballistic resistance of fractured ceramic systems. In this paper ceramic compacts with radically different initial morphologies, acting as comminuted ceramic analogues, were studied. Key experimental approaches, comprising both depth-of-penetration [1, 12, 13, 14] and shock-loading (plate-impact) [16, 17, 18] studies are introduced before presentation of experimental results. These results were also compared to re-interpreted data from a previous investigation [15]. Results from these complimentary sets of experiments reinforced each other, showing clear evidence of a contribution of particle morphology to subsequent ballistic response.

2. Experimental Setup

Ballistic experiments were performed on a series of cold-pressed alumina powder compacts using a 30-mm bore, 5-m barrel, single-stage gas-gun [19]. This was used to launch saboted 7.62-mm FFV (WC-Co cored) rounds into the target compacts. The impact velocities were measured using a combination of in-situ light gates and high speed video footage captured using a Phantom V7 camera. The WC-Co rounds were chosen due to their high strength / hardness, allowing penetration of the relatively weak Al backing blocks employed with minimal projectile deformation / erosion. Two different experimental configurations were considered, both employing targets comprised of cold-pressed commercially-sourced plasma

spray Al_2O_3 powders. In both cases the compacts were pressed into 70-mm diameter hollow dural (Al 6082-T651) cylinders with a 50-mm internal diameter. A 150 or 500 MPa press was employed as required, with the general approach shown in Fig. 1 followed in each case.
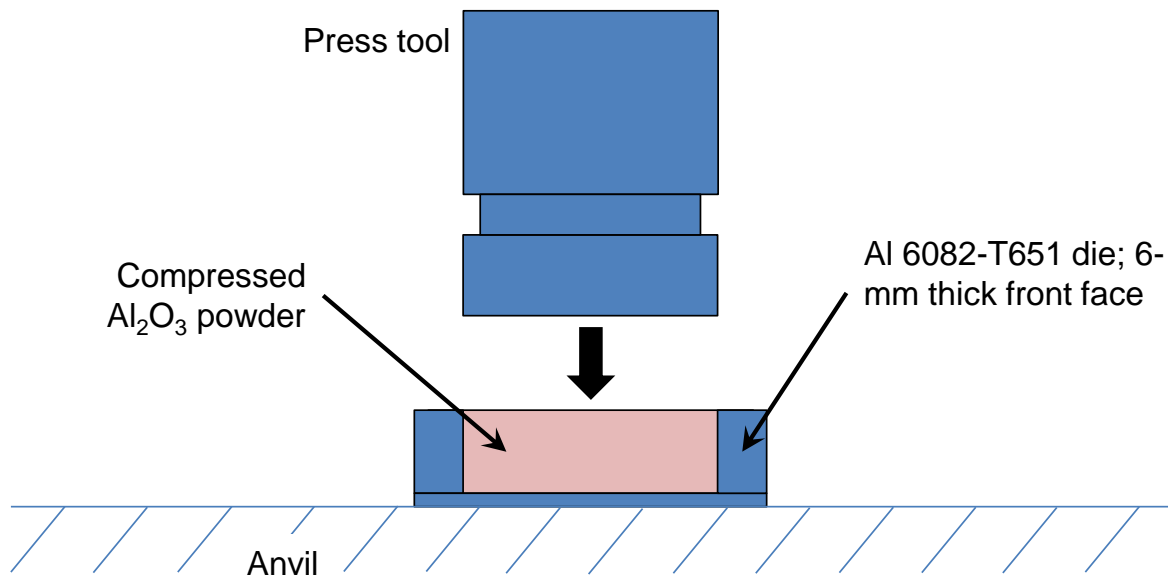

Fig. 1. Schematic illustration of pressing arrangement (target arrangement for experiment 1 shown).

The first set of experiments (building on results reported elsewhere for the angular 105NS material [15]) were designed to investigate the effects on ballistic performance of pressing pressure – and therefore resultant compact microstructure and density, whereas the second were focused on the influence of pressed sample thickness.

In the first set of experiments, 7.62-mm FFV rounds were accelerated at ~900 m/s into 6-mm Al fronted targets comprising of differing thicknesses of compacted alumina powder of one of two differing initial morphologies. These powders were compacted at 50, 150 or 350 MPa as-required, with the aim of generating differing initial compact microstructures via differing extents of powder compaction / interaction and fragmentation / wear during pressing.

Initially the target cups comprised a 30-mm space behind the 6-mm thick front Al face. This was filled with un-compressed powder which was then compressed as-required before being sealed in place with an epoxy layer, with the cup than machined down flush to the final compressed depth. For these experiments, given the relatively high thickness of the Al cover which would have led to significant jacket removal, partially pre-stripped rounds were employed to try and ensure full jacket removal before impact with the ceramic compact in order to avoid any influence of uneven jacket removal on subsequent ballistic response (such an approach is in-line with experiments conducted elsewhere by a selection of the authors [20]).

For the second set of experiments, a slightly different approach was adopted. These tests were designed to investigate the effect of changing pressed ceramic thickness (which was kept constant in the first set of experiments), with differing microstructures again accessed via the use of two different morphology ceramic powder feedstocks, although with only a single pressing pressure of 150 MPa employed. As a selection of pressed ceramic thicknesses were considered (4, 8 and 12-mm), it was inevitable that a higher proportion of targets would have lower thicknesses than in experiment 1. Consequently, a thinner 1-mm thick Al cover was employed compared to the thicker 6-mm cover in the previous set of experiments with the aim of minimising influence of the cover on the ballistic performance of the compact. In light of this approach, the decision was taken to use fully jacketed 7.62-mm FFV rounds for this series of tests as the cover thickness was judged insufficient to ensure stripping of the jacket, even if initially pre-stripped. Further, a slightly lower impact velocity of ~862 m/s was employed to increase projectile-ceramic interaction time and, consequently, the fidelity of measured depths-of-penetration following penetration of the relatively thin (as opposed to the first set of tests) ceramic compacts employed. This was considered a valid

approach as the impact velocity was known from the first experiment to be below the transition velocity for the pressed compacts, ensuring dwell would occur.

For clarity, a summary of key experimental variables where there were differences between the two approaches adopted is presented in Table 1 (with the approach for experiment 1 building on that described previously in Ref. [15] elsewhere).

Table 1. Target / cover plate configuration for experiments 1 and 2.

Variable	Experiment 1 (pressure)	Experiment 2 (thickness)
Projectile	7.62-mm FFV round; front 8-mm of core exposed → 899 ± 3 m/s	7.62-mm FFV round fully jacketed
Die front plate thickness / initial depth (mm)	6 / 30	1 / 4, 8 or 12 (as-required)
Ceramic powders investigated	105NS 6100	105NS 6100
Compaction approach	Initial fill to a set depth, followed by compaction at 50, 150 or 350 MPa as-required	Continual fill / pressing at 150 MPa until the die was filled to its machined depth (4, 8 or 12 mm)
Final target plate preparation	Compacted material sealed with epoxy followed by machining of surrounding Al cup lip to the compacted ceramic depth	----

The prepared compacts were epoxied to the impact face of a series of four Al 6082 witness

plates as shown in Fig. 2.

Al 6082-T651 die; 6-
mm thick front face

FFV round:
exposed core

Compressed
Al_2O_3 powder
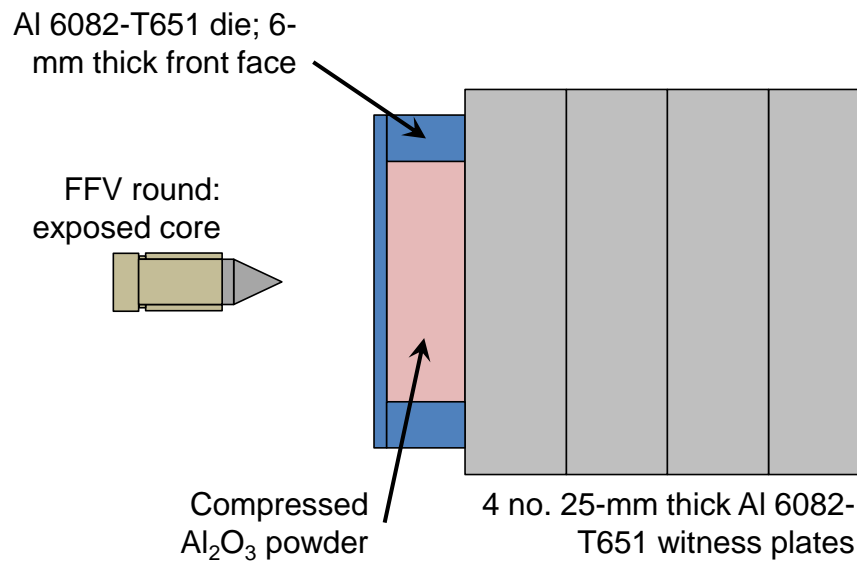
4 no. 25-mm thick Al 6082-
T651 witness plates

Fig. 2. Schematic illustration of experimental DOP target configuration for experiment 1.

Two differing powders were employed, both manufactured by Sulzer Metco; Metco 105NS

and 6100, the morphologies of which are shown in Fig. 3. Note the angular appearance and

the spherical morphology of the 105NS and 6100 powders respectively. Optical analysis

showed that Metco 105NS possessed a bi-modal particle size distribution centred on 15-20

and 30-35 microns, whereas the 6100 material had a more normal size distribution centred at
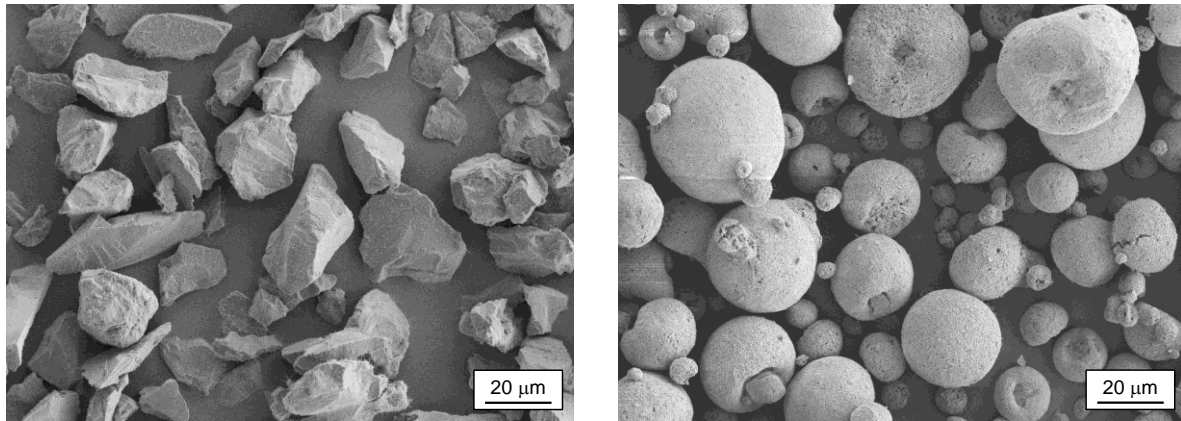
5-10 microns.

Fig. 3. Scanning electron micrographs of as-manufactured Al_2O_3 powders: (left) 105NS; (right) 6100.

In addition to the aforementioned ballistic tests, two plate-impact experiments [16, 17] were also undertaken. For these experiments the powders were pressed to 150 MPa in nominally 4.5-mm deep, 1-mm fronted Al 6082 hollow cylinders – with targets arranged as shown in Fig. 4. A 50-mm bore, single-stage gas-gun [21] was used to launch 10-mm thick Al 1050A impactors into these targets at ~570 m/s. A rear longitudinal manganin gauge (Vishay Micro-Measurements, USA, of type LM-SS-125CH-048) was employed in both cases, with this gauge isolated from the compressed ceramic puck / target via a 25 μm-thick Mylar^{TM} outer layer. Subsequent gauge interpretation to transform recorded voltages to stresses was based on the impedance matching technique [16] and following the approach adopted by Rosenberg et al. [22].
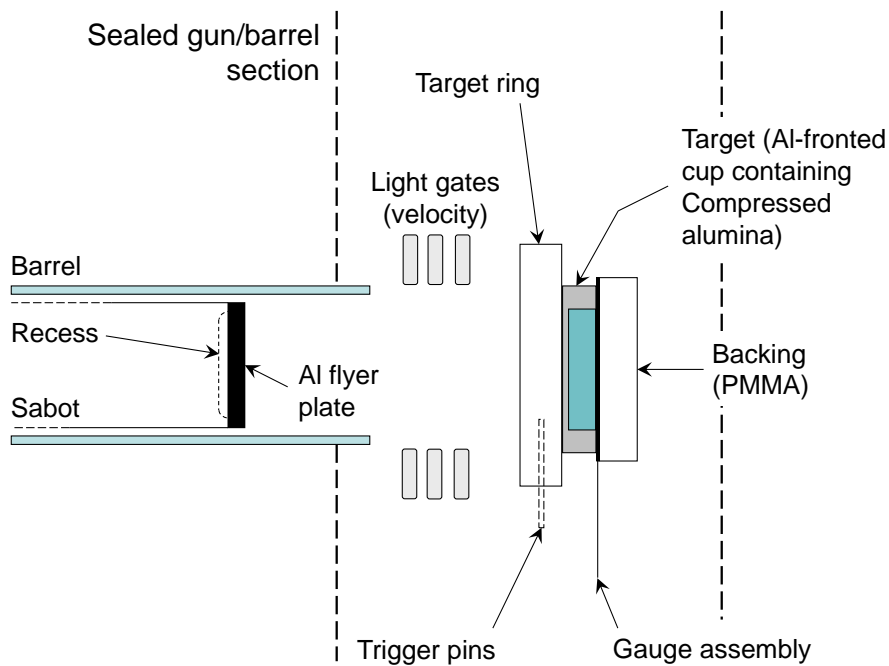
Fig. 4. Schematic illustration of the plate-impact experimental setup.

3. Results and Discussion

As discussed, for the ballistic experiments, the powders shown in Fig. 3 were pressed to 50, 150 and 350 MPa; whereas powders were pressed to 50 MPa only for the plate-impact experiments. The combination of different pressing pressures and initial powder morphologies was designed to access a number of different initial and final compact microstructure. When compressed to increased pressures, the 105NS material continued to exhibit an angular morphology, with some evidence of rounding of the granular edges as well as some flaking / trans-granular cracking at 150 MPa. In contrast, the originally spherical Metco 6100 was gradually flattened such that a laminar structure was likely developed in the compacts. Consequently, for a given feedstock powder, cold-pressing at different pressures led to different target puck microstructures, analogous to differing modes of ceramic armour pre-fragmentation. The effects of pressing to 150 and 350 MPa are shown in Fig. 5 where samples of pressed 105NS and 6100 are illustrated. In particular, it is worth noting the

gradual collapse of the apparently porous 6100 material – with flattened material in

compacted pucks subsequently forming (as shown by the close-up of such a structure in Fig.

5(d)), likely leading to a laminar microstructure once 350 MPa was reached. In the case of

the 105NS material, the effects of increased pressure are more subtle – with an enhanced

rounding of particle edges and (to a lesser extent) fracture of the particles apparent at 350
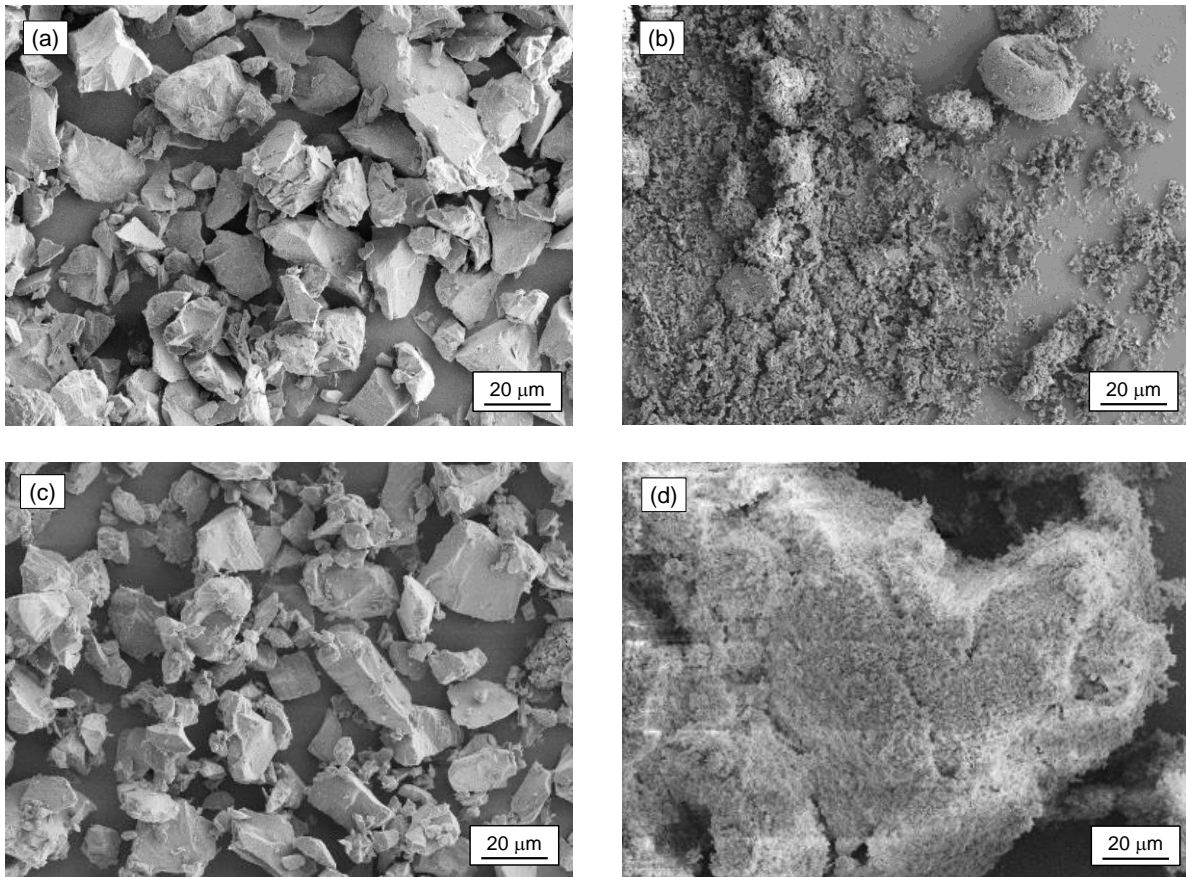
versus 150 MPa.

Fig. 5. Scanning electron micrographs of cold-pressed Al_2O_3 powders (in part adapted from Ref.

[15]): (a) / (b) pressed to 150 MPa and (c) / (d) to 350 MPa, for 105NS / 6100 respectively in each

case.

Experiment 1 comprised a total of twelve DOP tests; three shots employing powders pressed

to 50, 150 and 350 MPa as-discussed above (each repeated twice) for each of the two

powders under consideration. Following pressing the thickness of the resultant puck was

recorded, allowing calculation of the pressed volume (thickness $\times \pi \times$ [25 mm]^2); with any

13

G.J. Appleby-Thomas, D.C. Wood, A. Hameed, J. Painter, B. Fitzmaurice,

subsequent gap between the cup and powder being taken up during subsequent target assembly by a thin layer of epoxy. This allowed calculation of areal density (thickness × pressed density) for each puck [4]. Final depths-of-penetration were measured by sectioning the backing Al 6082 plates (this meant that any slight perturbations in the projectile path during penetration could be accounted for). In the case of experiment 2, a total of six tests were undertaken – 3 for each powder, with pressed powder target depths of 4, 8 and 12-mm respectively. In addition, for both tests a single shot was conducted into the Al backing only. Key experimental data is presented in Tables 2 and 3 for experiments 1 and 2 respectively. For comparison, the density of 99.8% Al_2O_3 is 3.8 g/cc[23]; whereas here, a peak density of 3.09 g/cc was obtained – meaning that even with a 350 MPa load, densities only reached ca 81 % of that for current ceramic armour material. Nevertheless, this is considered a realistic situation as the compacts are designed to represent comminuted (already impacted / pre-damaged) and confined – rather than fully compressed – ceramic armour material. Further, while not as effective an analogue as for pre-impacted material, the behaviour of the compacts considered here will likely provide a useful insight into the response of ceramic armour which has been pre-damaged by an elastic precursor on impact.

Table 2. Key experimental results for experiment 1.

Material	Pressing pressure (MPa)	Projectile impact velocity (m/s)	Pressed thickness (mm) / density (g/cc)	Measured DOP (mm):	E_m / η	E_m / η per unit KE (/kJ)
Al target only	----	899	-----	52.65 (excl. cover) 58.65 (incl. cover)	1.00 / ----	
105NS	50	901	9.17 / 2.22	45.26	0.99 / 6.79	0.330 / 2.25

	50	898	9.01 / 2.21	44.14	1.02 / 6.81	0.340 / 2.27
	150	894	8.56 / 2.38	44.29	1.01 / 6.67	0.341 / 2.24
	150	903	8.49 / 2.43	43.36	1.03 / 6.46	0.339 / 2.13
	350	901	8.39 / 2.47	43.93	1.02 / 6.50	0.337 / 2.15
	350	894	8.24 / 2.46	43.07	1.04 / 6.55	0.348 / 2.20
6100	50	897	8.30 / 1.57	46.79	1.02 / 10.96	0.339 / 3.66
	50	899	8.56 / 1.49	48.96	0.98 / 11.61	0.326 / 3.85
	150	899	7.14 / 1.84	45.97	1.03 / 10.68	0.343 / 3.55
	150	899	7.16 / 1.80	46.08	1.03 / 10.91	0.343 / 3.62
	350	902	4.16 / 3.09	46.99	1.02 / 11.13	0.335 / 3.67
	350	897	4.28 / 2.91	46.00	1.04 / 11.29	0.346 / 3.77

Table 3. Key experimental results for experiment 2.

Material	Pressing pressure (MPa)	Projectile impact velocity (m/s)	Pressed thickness (mm) / density (g/cc)	Measured DOP (mm):	E_m / η	E_m / η per unit KE (/kJ)
Al target only	----	862	----	42.57		0.325 / ----
				(excl. cover)	1.00 / ----	
				43.57		
				(incl. cover)		
105NS	150	868	4 / 2.33	42.43	0.93 / 12.59	0.299 / 4.05
	150	880	8 / 2.19	27.12	1.26 / 4.34	0.393 / 1.36
	150	874	12 / 2.37	22.67	1.27 / 2.24	0.403 / 0.71
6100	150	812	4 / 1.74	35.11	1.13 / 14.03	0.413 / 5.15
	150	862	8 / 1.81	31.25	1.16 / 6.01	0.377 / 1.96
	150	874	12 / 1.77	31.92	1.07 / 4.20	0.339 / 1.33

As detailed in Tables 2 and 3, two different measured of ballistic efficiency used elsewhere in the literature were employed. These were effective (ballistic) mass efficiency (E_m) [4, 24] and ballistic efficiency (η) [1]. Values were calculated using modified versions of equations from the literature based on recorded depth-of-penetration data, following Eqs. (1) and (2) respectively. Both equations normalise for pressed ceramic density (via the inclusion of areal density terms). In this manner, these equations therefore allow for differences in pressed compact density resulting from different packing densities. By definition, values of $E_m > 1$ represent an improvement in mass efficiency, whereas smaller values of η (e.g. below that of the baseline setup) represent an increase in ballistic efficiency. While E_m arguably represents a more complete assessment of ballistic performance (as the performance of the backing material only for a given depth-of-penetration test is accounted for), calculation of this value – as shown in Eq. (1) – is heavily weighted towards the ballistic properties of the backing (with this appearing on both the numerator and denominator). Consequently, if – as proved to be the case in the study contained herein – the introduced amour is relatively weak – meaning that large resultant DOPs are recorded, then there will inevitably be little variability in calculated E_m values. To this end, while η in Eq. (2) does not include the contribution of the baseline material with no covering ceramic – meaning data will not be fully normalised for total presented mass – it provides a much simpler and accessible measure of ballistic performance. Essentially, η measures the ratio of the areal density of material penetrated to armour presented. In this way, both backing (including cover plate in this case) and ceramic areal densities are accounted for. Further, while use of thicker ceramic plates would reduce values of η, this would be balanced by a corresponding decrease in residual penetrator (P_r). Overall, this means that η provides a relative measure of armour performance (smaller values corresponding to more efficient armour). Importantly, as all backing material penetration terms are now in the numerator only (as opposed to Eq. (1) for E_m), this means that η, as

calculated from Eq. (2) [1], will likely be significantly more sensitive to the performance of weaker armour materials such as comminuted ceramics.

$$E_m = \frac{p_{Al}(P_{Al-only} + t_{cover})}{\rho_0 t_{compact} + \rho_b(P_r + t_{cover})} \qquad (1)$$

$$\eta = \frac{\rho_{areal}^{Al}}{\rho_{areal}^{Ceramic}} = \frac{\rho_{Al}(P_r + t_{cover})}{\rho_0 t_{compact}} \qquad (2)$$

Where ρ_b and ρ_0 are the density of the Al backing / cover and as-pressed ceramic compact; $P_{Al-only}$ and P_r are the penetration into the backing plate (with cover present but no powder) and residual penetration into the backing Al when a ceramic compact was present respectively, and; $t_{compact}$ and t_{cover} are the thickness of the as-pressed powder compact and Al front cover plate respectively.

Due to the differing range of ceramic thicknesses compared, experimental results from the two different tests have largely been considered separately.

4. Experiment 1: Effects of Pressing Pressure

As noted previously, differing pressing pressures led to variations in the resultant compact. Consequently, the experimental results from this set of tests are presented in terms of the variation in key ballistic properties with pressing pressure – itself representative of differing underlying material microstructures. The variations of E_m and η with ceramic pressing pressure (from Table 2) are presented in Figs. 6(a) and (b) respectively.
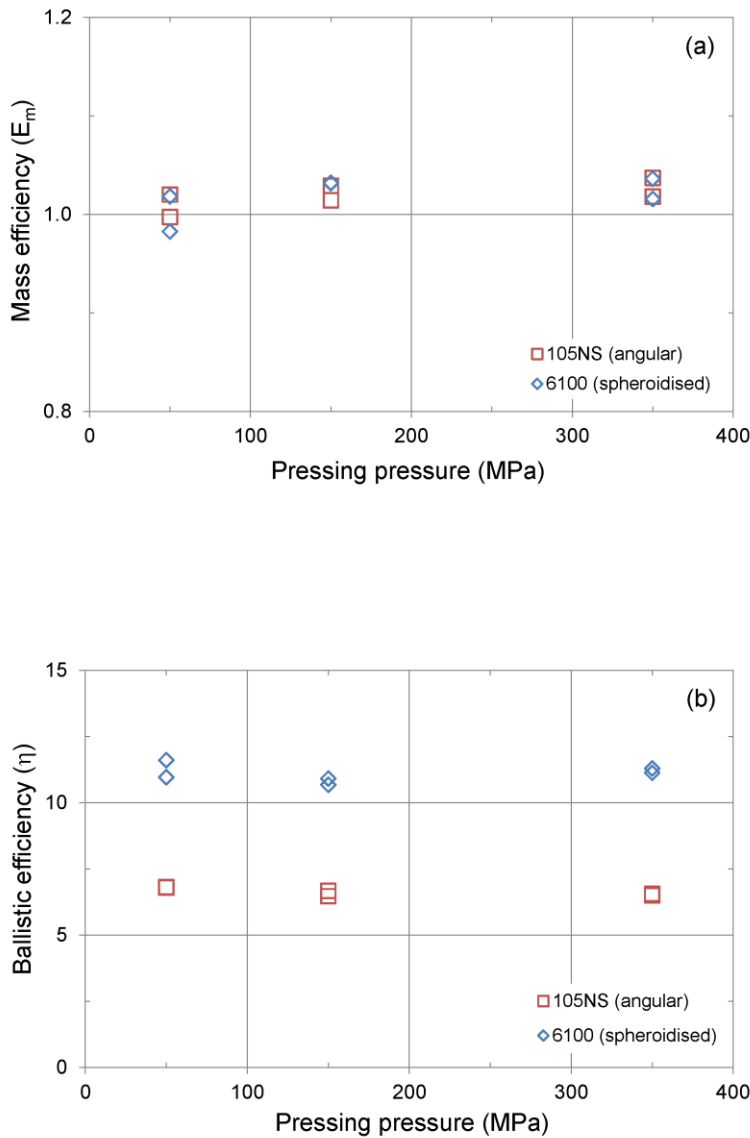
17

Fig. 6. Variation of mass (a) and ballistic (b) efficiency with pressing load for experiment 1.

Several observations may be drawn from Fig. 6. In terms of mass efficiency, Fig. 6(a) shows that there is little separation between the experimental data points for the 105NS and 6100 materials. However, in both cases there seems to be a general trend towards a more mass-efficient solution at higher pressing pressures (presumably as the compressed material becomes more consistent and closer to a fully dense compact in makeup). Overall, however, as detailed in Table 2, mass efficiency is relatively low at just above unity. This fact,

consistent with a previous study into 105NS [15], may suggest that the pressed thickness was too high to be a weight-efficient ballistic solution. However, as detailed in Fig. 7(a) later, the mass efficiency of similar pressed thicknesses in experiment 2 was significantly higher – suggesting that the different experimental conditions in this first test, highlighted in Table 1, influenced the relatively low E_m values in Fig. 6(a).

In contrast to the discussion above, the ballistic efficiency (η) shown in Fig. 6(b) exhibits a clear difference between the behaviour of the 105NS and 6100 materials. As with the E_m data in Fig. 6(a), η values for the 6100 material become more consistent / show less local scatter in differing experimental data-sets at higher pressures; however, the scatter in the data for the NS105 material is consistently similar at all pressures. However, in Fig. 6(b) the 105NS material shows a significantly greater ballistic efficiency (smaller values of η in line with Eq. (2)) than the 6100 material at all pressing pressures. This strongly suggests, in line with results from Horsfall et al. [11], that a ballistic resistance advantage has arisen due to the underlying angular material microstructure. While it is worth noting that in all cases the discussion above is based on only a limited number of data points, the presence of underlying trends (e.g. variation of mass and ballistic efficiency with pressing pressure in Figs. 6(a) and (b) respectively) strongly suggests that observed behaviour has an underpinning physical explanation. In line with this conclusion, such a result in terms of a link between compact properties and subsequent response under load is consistent with the well-known phenomena of steric hindrance [25, 26]. Essentially, it is tentatively postulated that frictional interaction of the angular particles within the 105NS-based compacts leads to greater resistance under compression (here, ballistic attack) than is the case with the 6100-based targets.

Building on the discussion above, while underlying particle / compact morphology clearly had a marked effect on the ballistic efficiency values (η) presented in Fig. 6(b), this was not

the case for the mass efficiency values in Fig. 6(a). Essentially, as shown in Eq. (1), calculation of E_m is strongly dependant on the properties of the case and backing – whereas for η, as highlighted in Eq. (2), the relative performance of the backing and cover plate are not included – bringing the contribution of the ceramic material itself to the fore. Consequently in experiment 1, it seems likely that the 6-mm thick front face dominated the target ballistic performance (despite the use of pre-stripped rounds); whereas in experiment 2 the thinner cover plate led to a more marked variation with underlying target compact morphology (e.g. Fig. 7).

5. Experiment 2: Effects of Compact Thickness

The variation of E_m and η with pressed ceramic compact thickness is presented in Figs. 7(a) and (b) respectively. Further, data for the comparable 150 MPa pressed material from experiment 1 (Table 2) is also included for comparison.
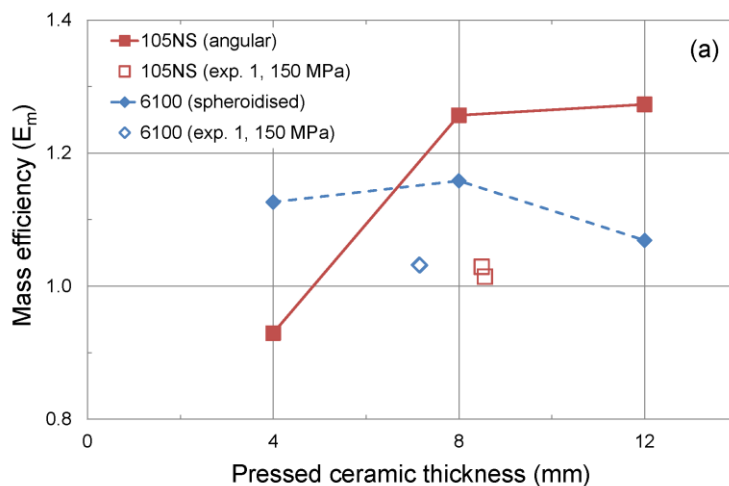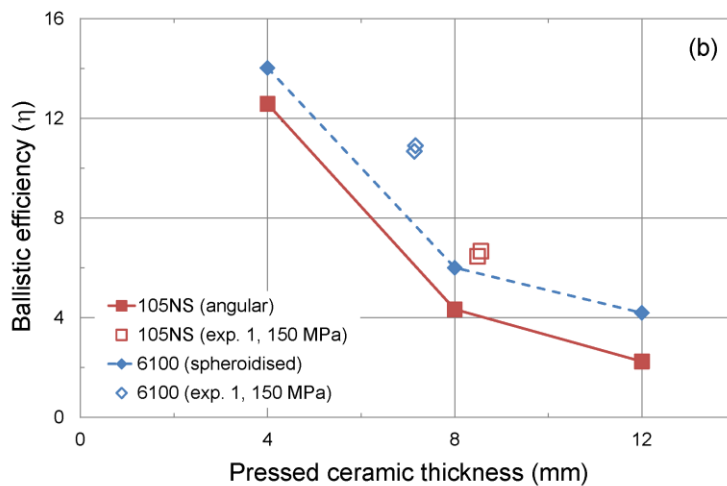
Fig. 7. Variation of mass (a) and ballistic (b) efficiency with pressed ceramic thickness for experiment 2 from Table 3 (plus data from experiment 1 / Table 2, shown in open symbols, for compacts pressed to 150 MPa).

The mass efficiency for both the angular (105NS) and spheroidized (6100) feedstock compacts shown in Fig. 7(a) for experiment 2 is consistently greater than unity for all bar the lowest thickness 105NS case. This is in marked contrast to the data for experiment 1, where E_m values were only just above unity – e.g. the introduction of the ceramic compact leads to a armour which is consistently more mass efficient than the backing Al alone. This backs the assumption made earlier that the relatively poor performance of the pressed compacts considered in experiment 1 was a function of the experimental conditions (likely the thicker target cover employed for those tests over experiment 2 – although the higher average impact velocity detailed in Table 3 may also have had an influence). For the apparently anomalous (lowest thickness) data point from experiment 2 the impact velocity was relatively low compared to other shots; e.g. just 812 m/s compared to approximately 870 m/s in all other cases. For interest, values of E_m and η normalised by impact kinetic energy are also included

in Tables 2 and 3; these E_m / KE values may be shown to follow a similar pattern to those for the un-normalised values of E_m presented in Fig. 7(a). When combined with the fact that the shots presented here for experiment 1 were conducted at approximately 900 m/s, this inconsistency with the apparent trends for the majority of (similar velocity) data for the anomalous data point (as well as the difference between experiment 1 and 2 data for otherwise similar ceramic thicknesses) suggests that impact velocity (e.g. rate of material loading) has an effect on ballistic efficiency for these compacts. Such a result would be consistent with the postulation that frictional interaction between comminuted material elements is key to ballistic performance in comminuted ceramics.

Overall, for the higher thicknesses (> 4 mm) compacts, the angular feedstock 105NS material appeared to present higher (and therefore more efficient) E_m values than the 6100 targets. While based on the use of single data points at a given pressing pressure, as touched on in the description of experiment 1, it is argued that the existence of these general trends in both materials suggested an underlying physical mechanism governing material response. Further, the data presented in Fig. 7(a) tentatively suggests that the 105NS targets became more efficient at higher pressed thicknesses as opposed to the 6100 material which showed a general decline in mass efficiency. The difference, while admittedly based on only a handful of data points, was most marked at a thickness of ~12 mm, with the 105NS material demonstrating a mass efficiency value approximately 19% higher than that of the corresponding spherical-feedstock 6100 target. While further data would be required to fully elucidate the tentative potential trends identified here, it is apparent that mass efficiency changes with both powder type (morphology) and pressed ceramic thickness.

This apparent morphological dependence of ballistic performance was also reflected in the ballistic efficiency (η) data presented in Fig. 7(b), where two different effects are apparent in

line with the corresponding E_m data. The first trend observed in Fig. 7(b) is that the angular material consistently demonstrated an enhanced ballistic efficiency value at all pressed thicknesses considered compared to the spherical-feedstock 6100 compacts. Secondly, there appears to be evidence of a thickness effect, in that an apparent trend toward a plateau in terms of ballistic efficiency is observed at elevated target thicknesses. In addition, despite differing experimental conditions, the 150 MPa data from experiment 1 included in Fig. 7(b) appears to follow a similar trend, supporting the assumption that the difference in cold-pressed compact ballistic response may be based on initial feedstock morphology.

Overall, both of the results presented in Fig. 7 seem to back the concept that comminuted material morphology may strongly effect the ballistic response of a fractured ceramic system. From experiment 1, compacts based on angular materials appear consistently more ballistically efficient than those constructed from spheroidal feedstock material. Referring to Fig. 8, it is proposed that the mechanisms governing the greater resistance to penetration in the case of the 105NS compacts – Fig. 8(a) – arises due to frictional interaction between the individual angular powder grains. Whereas with the more spheroidized 6100 targets, shown in an arbitrary semi-collapsed state as a result of cold compression in Fig. 8(b), the enhanced ability of the powder particles to collapse under load leads to greater deformation / less resistance to penetration than with the angular feedstock material.
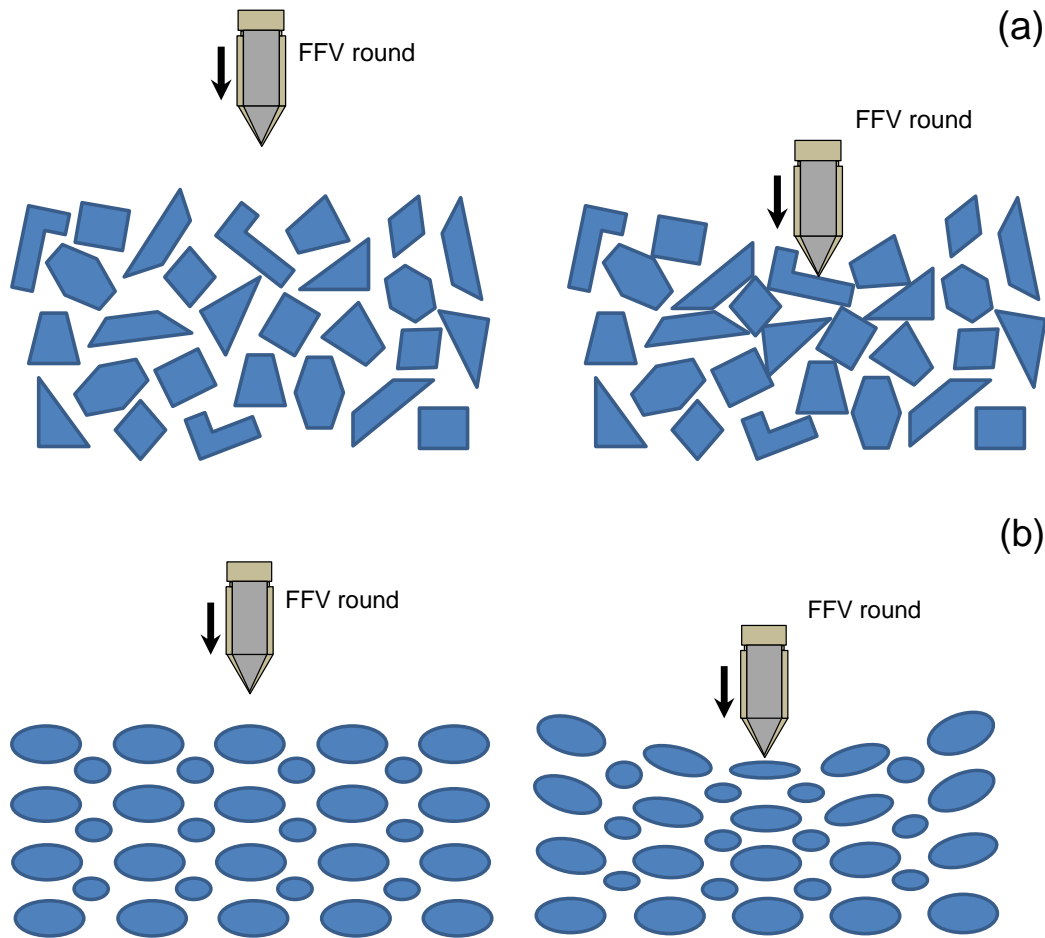
Fig. 8. Schematic illustration of proposed differences in Metco pressed ceramic powder response during ballistic impact: (a) 105NS; (b) 6100.

6. Plate-Impact Experiments

The influence of ceramic morphology in terms of comminuted material response was also investigated via a pair of plate-impact experiments [16, 17, 18], following the approach shown in Fig. 4, with the general aim of studying how the presence of differing target materials / compacts modified an initially planar shock. While acknowledged that a shock wave would not be established for any significant distance ahead of a penetrating bullet in a ceramic target, this experiment was carried out in order to elucidate the way in which a well-defined planar input wave was modified on passage through differing target materials. It is

well known that multi-phase materials [17] – and in particular granular materials [27, 28] – can, under such impact conditions, undergo complex loadings. Here, both experiments occurred at a measured impact velocity of 567 m/s (±5 m/s). Consequently based on a longitudinal sound speed (c_L) value of nominally 6.38 mm/μs for Al 1100 [29], and the use of 10-mm thick Al 1050A flyers it was calculated that releases from the rear of the flyer would not re-enter the main target until ~3.3 μs after impact. Further, given the high sound speeds in alumina (e.g. c_L values of ~10 mm/μs), as well as the relatively high pressed densities here, release waves from the rear of the flyer will certainly not have caught up with the shock in the thinnest – nominally 4.5-mm thick – powder compacts until > 4 μs after initial shock arrival at the rear gauge. The resultant gauge traces, shifted in time to show shock arrival ca 1 μs in each case, are presented in Fig. 9. It's worth noting that, in line with the discussion above, the duration of these traces, at approximately 3 μs, is such that the system can reasonably be expected to have remained in a state of one-dimensional strain for the duration of the experiment.
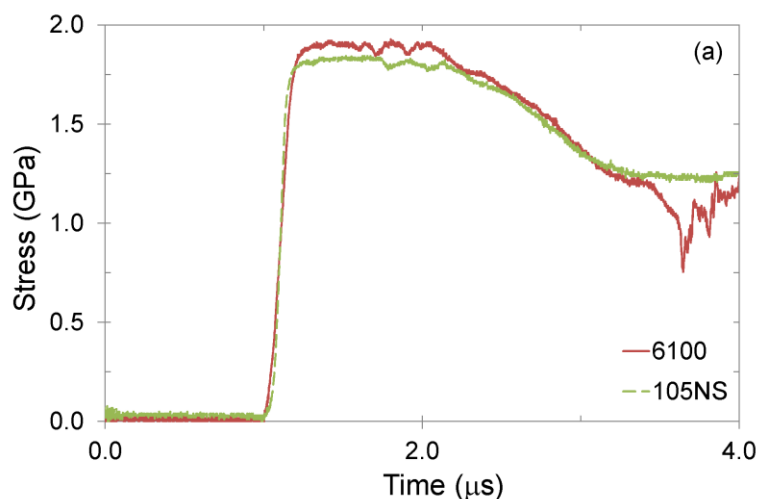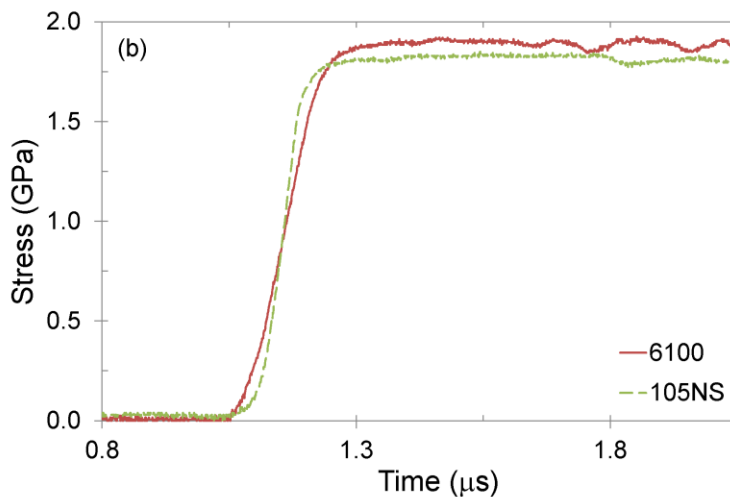
Fig. 9. Rear surface manganin gauge traces illustrating the effect of shock passage through Metco 105NS and 6100: (a) full data including release; (b) shock arrival and initial plateau only.

As shown in Fig. 9, the 6100 and NS105 materials reached relatively similar peak stresses of 1.93 and 1.84 GPa respectively. This slight difference in peak stress (~4.7%) is likely attributable to a combination of the following factors: (1) small differences in flyer impact velocity (as detailed previously, errors of ±5 m/s are estimated here); (2) the difference in initial pressed densities of the different powder compacts. In particular, in the latter case, where (as shown in Tables 2 and 3) the pressed densities at 150 MPa of the 105NS material (2.34 ± 0.10 g/cc) were consistently around 30% higher than those of the 6100 material (1.80 ± 0.04 g/cc). Consequently, a combination of the lower initial density of the 6100 material and the likely enhanced packing resulting from the initially spherical (and, as shown in Fig. 5, post-compression, laminar) structure, might be expected to lead to a higher peak stress under otherwise identical loading conditions as the 6100 material could potentially reach a greater peak density than the 105NS sample – in-line with Fig. 9. To this end, this slight difference in peak stress is likely a function of initial powder packing density; however, the fact that

26

both traces do not converge also suggested that peak theoretical density is not obtained at the nominal loadings encountered here. In addition to the small difference in peak stress, a notable difference also exists between the rise times for the two powders under consideration. As shown in detail in Fig. 9(b), the angular 105NS target material exhibits a much steeper rise – whereas the (initially) spheroidized 6100 material shows a more ramped response on shock arrival. From Fig. 9(b), total rise-time for the 105NS material was 185 ns as opposed to 249 ns for the 6100 material – whereas for comparison, typical gauge rise times are found to be <100 ns due to the fact that the gauge thickness is ~50 μm, with an insulating Mylar^{TM} layer of just 25 μm [17]. This difference in rise time to the main plateau therefore equates to approximately 26%. It should be emphasised that ~~s~~ such a difference may well be attributable to alignment issues or even factors such as a small air gap between the gauge and powder compact. However, great care was taken to avoid such issues – in particular, on construction, a slow-curing epoxy was employed to bond the powder compact to the gauge, with the flow of this epoxy over time designed to fill any such gaps. Consequently, while care must be taken in gauge interpretation – not least when subjected to a non-linear ramp-type loading as discussed here – it is suggested in his instance that this result is consistent with the idea that the lower initial density 6100 compact is continuing to collapse for a longer period under shock loading. Whereas, in contrast, it is postulated that the more-angular 105NS particles lock together more rapidly, providing greater resistance to compression and a correspondingly faster rise to peak stress. While necessarily only a postulation – not least given the fact that results from just two experiments are presented here – such behaviour is consistent with the model of the bi-phase material WC-Co collapsing presented elsewhere by a selection of the current authors [17], where identification of a multi-phase Hugoniot equation-of-state strongly suggested that after collapse of the initial weaker Co phase, the angular WC particles interlocked, leading to a strengthening and secondary-phase in the

loading profile. Consequently, it is tentatively suggested that this proposed morphological model arguably backs the discussion of the ballistic experimental results presented in Figs 6 and 7 / summarized in Fig. 8, where it was suggested that the apparently enhanced ballistic response of the 105NS material was a function of such particle interaction under loading.

7. Conclusions

A series of depth-of-penetration experiments have been conducted using comminuted ceramic analogues comprising cold-pressed ceramic compacts manufactured from pure alumina feedstock materials of differing initial morphology to investigate the influence of material morphology on ballistic strength. Two measures of ballistic resistance were considered; effective (ballistic) mass efficiency – which took into account the entire armour and backing areal density, and ballistic efficiency – which neglected the influence of the armour packaging – but which in turn emphasised the relative performance of the ceramic compacts themselves. Overall, two key influences of compact construction on ballistic response were observed:

1) Initial compact morphology was found to have a measurable influence on ballistic response, in particular in terms of calculated ballistic efficiency, with targets manufactured from an angular feedstock found to exhibit the greatest ballistic resistance.

2) Under similar pressing pressures (e.g. with similar underlying microstructures), compact thicknesses were shown to have a marked effect on ballistic response – with ballistic efficiency in particular initially increasing, but appearing to plateau at higher target thicknesses.

Overall, while previous studies have touched on the concept, the results presented herein (in particular, ballistic efficiency data) have shown clear evidence that underlying fragment morphology has a marked influence on compact ballistic response. In particular, angular morphology feedstock material has been shown to lead to a notably more efficient (ballistically) 'comminuted ceramic simulant'. These results were backed by data from a small number of plate-impact experiments which suggested that angular feedstock materials impacted under otherwise similar conditions exhibited a greater resistance to loading than targets based on spheroidized material. This assumption was based on a notable modification of the initial rise of gauges recording the shock at the rear face of the target.

In conclusion, taken together, these experimental results should therefore serve to provide a useful baseline for further optimisation studies into this important field of residual ballistic performance of damaged / comminuted ceramics. In particular, this study appears to suggest that if ceramic armour failure could be controlled via careful control of underlying microstructure to provide angular fragments, ballistic performance of post-impact residual compact material could potentially be enhanced.

Acknowledgements

Figure Captions

Fig. 1. Schematic illustration of pressing arrangement (target arrangement for experiment 1 shown).

Fig. 2. Schematic illustration of experimental DOP target configuration for experiment 1.

Fig. 3. Scanning electron micrographs of as-manufactured Al2O3 powders: (left) 105NS; (right) 6100.

Fig. 4. Schematic illustration of the plate-impact experimental setup.

Fig. 5. Scanning electron micrographs of cold-pressed Al_2O_3 powders at 150 MPa: (left) 105NS; (right) 6100.

Fig. 6. Variation of mass (a) and ballistic (b) efficiency with pressing load for experiment 1.

Fig. 7. Variation of mass (a) and ballistic (b) efficiency with pressed ceramic thickness for experiment 2 from Table 3 (plus data from experiment 1 / Table 2, shown in open symbols, for compacts pressed to 150 MPa).

Fig. 8. Schematic illustration of proposed differences in Metco pressed ceramic powder response during ballistic impact: (a) 105NS; (b) 6100.

Fig. 9. Rear surface manganin gauge traces illustrating the effect of shock passage through Metco 105NS and 6100: (a) full data including release; (b) shock arrival and initial plateau only.

References

[1] Walley SM. Historical review of high strain rate and shock properties of ceramics relevant to their application in armour. Adv. in Appl. Ceram. 2010;109(8):446-466.

[2] Sternberg J. Material properties determining the resistance of ceramics to high velocity penetration. J. Appl. Phys. 1989;65(9):3417.

[3] John V. Introduction to Engineering Materials, 4th ed., Palgrave MacMillan, 2003.

[4] Hazell PJ. Ceramic Armour: Design and Defeat Mechanisms, Argos Press, 2006.

[5] Callister Jr WD. Materials Science and Engineering: An Introduction, 6th ed., John Wiley & Sons, Inc., 2003.

[6] Antoun T, Seaman L, Curran DR, Kanel GI, Razorenow SV, Utkin AV. Spall Fracture. Springer-Verlag, New York, USA, 2003, pp. 162-168.

[7] Nanda N, Appleby-Thomas GJ, Wood DC, Hazell PJ. Ballistic behaviour of explosively shattered alumina and silicon carbide targets. Adv. in Appl. Ceram. 2011;110(5), 287-292.

[8] Hazell PJ, Appleby-Thomas GJ. More on penetration of ceramic based targets by non-deforming projectiles. Adv. in Appl. Ceram. (2012);111(3):171-173..

[9] Bourne NK. On kinetics of failure in, and resistance to penetration of metals and ceramics. Adv. in Appl. Ceram 2010;109(8):480-486.

[10] Holmquist TM, Anderson Jr CE, Behner T, Orphal DL. Mechanics of dwell and post-dwell penetration. Adv. in Appl. Ceram. 2010;109(8):467-479.

[11] Horsfall I, Edwards MR, Hallas MJ. Ballistic and physical properties of highly fractured alumina. Adv. in Appl. Ceram. 2010;109(8):498-503.

[12] Rosenberg Z, and Yeshurun Y. The relation between ballastic efficiency and compressive strength of ceramic tiles. Int. J. Impact Engng. 1988;7(3), 357-362.

[13] Bless S. Using Depth-of-Penetration Tests to Design Transparent Armor. Exp. Mechanics 2013;53(1):47-51.

[14] Hazell PJ. Measuring the strength of brittle materials by depth-of-penetration testing. Adv. in Appl. Ceram. 2010;109(8):504-510.

[15] Hazell PJ, Appleby-Thomas GJ, Toone S. Ballistic compaction of a confined ceramic powder by a non-deforming projectile: Experiments and simulations. Mater. & Design 2014;56:943-952.

[16] Meyers MA. Dynamic Behavior of Materials, 2nd ed., John Wiley and Sons, 1994.

[17] Appleby-Thomas GJ, Hazell PJ, Stennett C, Cooper G, Helaar K, Diederen AM. Shock propagation in a cemented tungsten carbide. J. of Appl. Phys. 2009;**105(6)**:064916.

[18] Millett JCF, Whiteman G, Stirk SM, Bourne NK, Shear strength measurements in a shock loaded commercial silastomer. J. Phys. D: Appl. Phys., 2011;44(18):185403.

[19] Hazell PJ, Cowie A, Kister G, Stennett C, Cooper GA. Penetration of a woven CFRP laminate by a high velocity steel sphere impacting at velocities of up to 1875 m/s. Int. J. of Impact Engng. 2009;36(9):1136-1142.

[20] Hazell PJ, Appleby-Thomas GJ, Philbey D, Tolman W. The effect of gilding jacket material on the penetration mechanics of a 7.62 mm armour-piercing projectile. Int. J. of Impact Engng. 2013;54:11-18.

[21] Bourne NK. A 50 mm bore gas gun for dynamic loading of materials and structures. Meas. Sci. Technol. 2003;14(3):273-278.

[22] Rosenberg Z, Yaziv D, Partom Y. Calibration of foil-like manganin gauges in planar shock wave experiments. J. Appl. Phys. 1980;51:3702.

[23] Hazell PJ. Armour: Materials, Theory and Design, CRC Press, 2016.

[24] Rosenberg Z, Yeshurun Y, Tsaliah J. More on the thick-backing screening technique for ceramic tiles against AP projectiles, In: Proceedings of the 12th International Symposium on Ballistics, San Antonio, Texas, USA, Vol. 3, 1990. p. 197-201.

[25] Bourne NK, Millett JCF. On the influence of chain morphology on the shock response of three thermoplastics. Metallurgical and Mater. Trans. A: Phys. Metallurgy and Mater. Sci. 2008;39(2):266-271.

[26] Bourne NK, Millett JCF. Tacticity in shocked polymer hydrocarbons. J. of Mater. Sci. 2008;43(1):185-189.

[27] Vogler TJ, Lee MY, Grady DE. Static and dynamic compaction of ceramic powders. Int. J. of Solids and Struct. 2007;44(2):636-658.

[28] Fredenburg DA, Koller DD, Coe JD, Kiyanda CB, The influence of morphology on the low- and high-strain-rate compaction response of CeO_2 powders. J. of Appl. Phys. 2014;115:123511.

[29] Marsh SP. LASL Shock Hugoniot Data, University of California Press, 1980.